Optical Engineering

OpticalEngineering.SPIEDigitalLibrary.org

Underwater three-dimensional imaging laser sensor with 120-deg wide-scanning angle using the combination of a dome lens and coaxial optics

Masaharu Imaki
Hideaki Ochimizu
Hidenobu Tsuji
Shumpei Kameyama
Takashi Saito
Shojiro Ishibashi
Hiroshi Yoshida

SPIE.

Masaharu Imaki, Hideaki Ochimizu, Hidenobu Tsuji, Shumpei Kameyama, Takashi Saito, Shojiro Ishibashi, Hiroshi Yoshida, "Underwater three-dimensional imaging laser sensor with 120-deg wide-scanning angle using the combination of a dome lens and coaxial optics," *Opt. Eng.* **56**(3), 031212 (2016), doi: 10.1117/1.OE.56.3.031212.

Underwater three-dimensional imaging laser sensor with 120-deg wide-scanning angle using the combination of a dome lens and coaxial optics

Masaharu Imaki,[a,*] Hideaki Ochimizu,[a] Hidenobu Tsuji,[a] Shumpei Kameyama,[a] Takashi Saito,[b] Shojiro Ishibashi,[c] and Hiroshi Yoshida[c]
[a]Mitsubishi Electric Corporation, 5-1-1 Ofuna, Kamakura, Kanagawa 247-8501, Japan
[b]Mitsubishi Electric Tokki Systems Corporation, 730-11 Kamimachiya, Kamakura, Kanagawa 247-0065, Japan
[c]Japan Agency for Marine-Earth Science and Technology, 2-15 Natsushimacyo, Yokosuka, Kanagawa 237-0061, Japan

Abstract. We developed an underwater three-dimensional (3-D) imaging sensor using a 532-nm laser. The sensor system combines a dome lens with coaxial optics to realize a wide-scanning angle of 120 deg (horizontal) × 30 deg (vertical) while having a compact size of 25-cm diameter and 60-cm length. A detector sensitivity time control circuit and a time-to-digital converter are used to detect a small signal and suppress the unwanted backscattered signals due to marine snow. 3-D imaging of the seafloor with 20-m width and 60-m length was demonstrated in the sea around Ishigaki Island, Japan. [DOI: 10.1117/1.OE.56.3.031212]

Keywords: underwater imaging; ranging; time-of-flight.

Paper 161076SSP received Jul. 7, 2016; accepted for publication Oct. 12, 2016; published online Oct. 28, 2016.

1 Introduction

Detailed three-dimensional (3-D) imaging of the surface of the seafloor is essential for underwater exploration.[1,2] Currently, the most widely used technology for exploration is sound navigation and ranging (SONAR), because acoustic waves can propagate through a long distance in water. However, SONAR suffers from unwanted multipass echoes that are due to reflections from the surrounding terrain. Thus, high-resolution underwater imaging using SONAR is difficult.

Alternatively, 3-D imaging on the surface of the seafloor has been proposed using laser-based structured light[3–6] and time-of-flight (TOF)[7–10] techniques. In these sensors, unwanted multipass signals are greatly reduced since the laser beam exhibits high directivity. Thus, high spatial resolution can be more easily achieved in 3-D imaging using these laser-based approaches.

In particular, 3-D imaging by structured light is advantageous because it reduces the influence of backscattering signals from marine snows. On the other hand, for long distance measurements, a minimum distance between the receiver and transmitter is necessary, which can be problematic in practice, especially if a compact design is required. The measurement distance and accuracy depend on the distance between the receiver and transmitter.

On the other hand, TOF methods can overcome this issue and result in a compact design. In particular, a more compact design is possible using a coaxial setup. Furthermore, undesired signals from marine snows can be discriminated from the desired signal from the seafloor using TOF information. Finally, obtaining high measurement precision at a long distance only depends on obtaining a sufficiently high signal-to-noise ratio (SNR), and not on the distance between the transmitter and receiver.

These factors, i.e., compactness, reduction of signals from marine snows, and relatively long-range imaging, are essential for seafloor exploration with autonomous underwater vehicles (AUVs) and remotely operated vehicles (ROVs). However, the main issue with conventional TOF sensors is their narrow sensor field-of-view (FOV), caused by a flat laser window. The window size is limited by underwater pressure resistance requirements. For this reason, Refs. 7–10 limit the scanning angle of the laser beam to 30 deg. In contrast, we demonstrate a scanning laser sensor for underwater 3-D imaging with a wide-scanning angle of 120 deg × 30 deg and compact size of 25-cm diameter and 60-cm length.

2 Sensor Architecture

Figure 1(a) shows the block diagram of the system. The transmitter is a 532-nm pulsed laser with a peak power of 5 kW, pulse width of 1 ns, and repetition rate of 50 kHz. We use the blue-green laser wavelength region because that wavelength has high transmittance in the water. The laser beam is transmitted to the seawater through the dome lens which has an inner diameter of 15 cm. The beam is scanned in a region of 120 deg (horizontal) × 30 deg (vertical) by a horizontal polygon scanner with vertical tilting, and the scanning speed of both directions is variable. The reflected light from the target is received through the dome lens and the polygon scanner and focused into a microchannel plate photomultiplier tube (MCP-PMT) which has a 250-ps rise time response. The true spatial resolution is determined by one of (1) beam divergence, (2) beam size at the sensor output, (3) angle spacing of transmitting beam spot, and

*Address all correspondence to: Masaharu Imaki, E-mail: Imaki.Masaharu@dc.MitsubishiElectric.co.jp

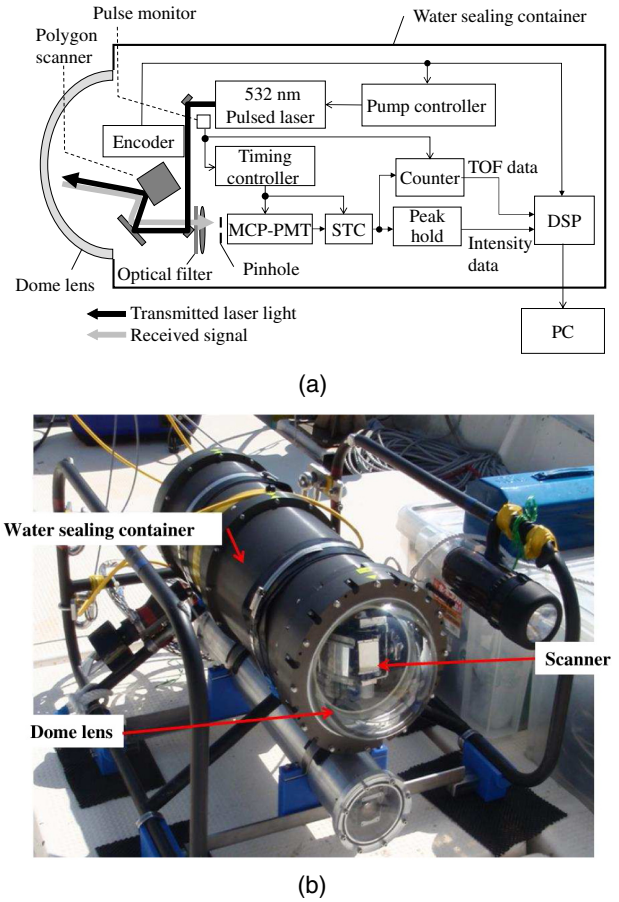

Fig. 1 The configuration of the system: (a) a block diagram and (b) a photograph.

(4) instantaneous FOV (IFOV). If the distance to the target is short or the water is clear, one of (1)-(3) determines the true spatial resolution. In the cases of turbid water especially for longer target distance cases, the backscattering in the water degrades the spatial resolution and the IFOV determines the resolution in many cases. The beam divergence is 0.002 deg, the beam size at the sensor output is 10 mm, and the angle spacing of the transmitting beam spot is 0.3 deg (horizontal) and 1 deg (vertical). The IFOV of the receiving optics is 1.2 deg respectively.

The received signals are compensated using a sensitivity time control (STC) circuit in which the reception gain is increased according to the TOF in order to compensate the attenuation effect of the signal intensity in the water. Subsequently, the TOF and the received signal intensity—which correspond to target distance and target reflectance—are measured by the counter and the peak hold circuit. The peak hold circuit is the simple capacitor type. A digital signal processor generates the system clock to control the system components, stores the TOF and intensity data of each frame, and transports them to a personal computer via a local area network. The container has pressure resistance for a water depth of 500 m and a size of 25-cm diameter and 60-cm length.

The sensor has several desirable features. In particular, a wide-scanning angle, combined with the pressure resistance and compactness of the sensor, is realized by appropriately configuring the dome lens and coaxial transmitter and receiver optics. Here, the reflective index of the seawater at 532-nm wavelength is extrapolated with 1.335, since the index at 486 nm is 1.3371 and 589 nm is 1.333.[11] If a flat window is used instead of a dome lens, the sensor FOV is limited to ±50 deg by the critical angle of the received light. This limitation can be negligible using the dome lens, and a wide beam scanning is possible. In this system, the 120 deg of horizontal angle is scanned using a polygon mirror. The 30 deg of vertical angle is scanned by tilting the polygon mirror in a direction perpendicular to the polygon rotating direction. However, there exists a strong internal reflected light from the dome lens, which can cause damage to the MCP-PMT or is blind up to a minimum range. To avoid this issue, we designed the scanning center of the transmitting beam to be slightly shifted from the center of the dome lens and set a pinhole before the focus position of the MCP-PMT. Figure 2 shows the details of the dome lens, the transmitter, and the receiver optics. The optical design requirement of the offset between the transmitter and the receiver is expressed by

$$d > \frac{DR}{2f}, \tag{1}$$

where d is the value of the scanner offset, D is the diameter of the pinhole, R is the radius of dome lens, and f is the focal length of the receiver lens. In this system, the scanner offset d is 8 mm, given the 1-mm diameter of the pinhole, 76-mm radius of dome lens, and 50-mm focal length. The scanning angle width of the transmitted beam in the water is equal to

$$\theta < \theta_a + \frac{d}{R}\left(1 - \frac{1}{n}\right) \sin\,\theta_a, \tag{2}$$

where θ_a is the scanning angle width of transmitting beam in the air, θ is the scan angle width of the transmitting beam, and n is the refractive index of seawater.

The laser output is controlled by a pump controller. Under certain conditions, the reflected light from the polygon scanner might be directly received by the MCP-PMT. In those cases, the photocathode surface of the MCP-PMT could be damaged. To avoid this issue, the pump controller stops the laser output when the scan angle is outside 120 deg.

The STC circuit amplifies the received signals to compensate the attenuation effect of the water. Figure 3 shows the concept of its function. In the case of turbid water, the received signal from the seafloor becomes smaller than the signal from suspended solids, water molecules, and marine snows near the system. The STC circuit changes the reception gain according to the TOF in a way that corresponds to the attenuation due to the water. By this function, the dynamic range of the received signal is equivalently enlarged. Furthermore, the ability to perform small signal detection—and consequently, the ranging distance—is improved. In our system, the STC has eight gain curves, and we can select the gain curve in accordance with the turbidity of the measurement environment. Figure 4 shows these gain curves.

The counter in this system might receive multiple signals. In this system, we use a commercially available time-to-digital converter (TDC) counter. Its time resolution is 27 ps and measurement range is up to 40 μs. The TDC has multiple (32 at maximum) pulse detection capabilities. Thus, the signal

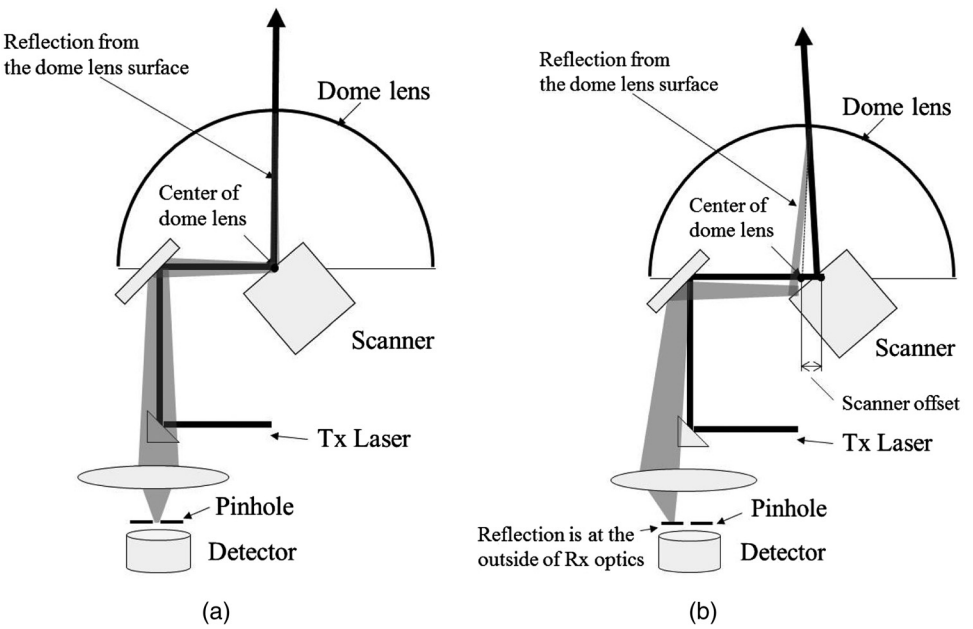

Fig. 2 Schematic of the reflected light from the dome lens: (a) without scanner offset and (b) with scanner offset.

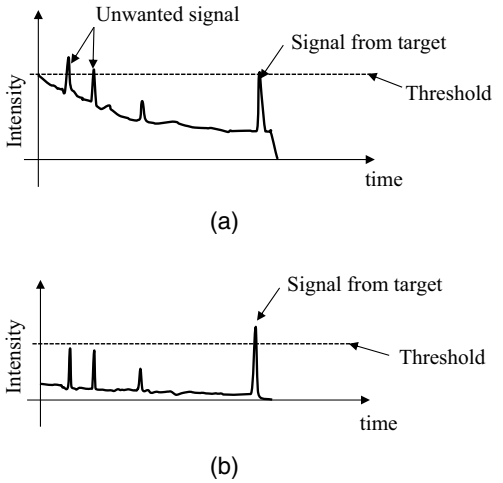

Fig. 3 Schematic of the function of STC: (a) before applying the STC and (b) after applying the STC.

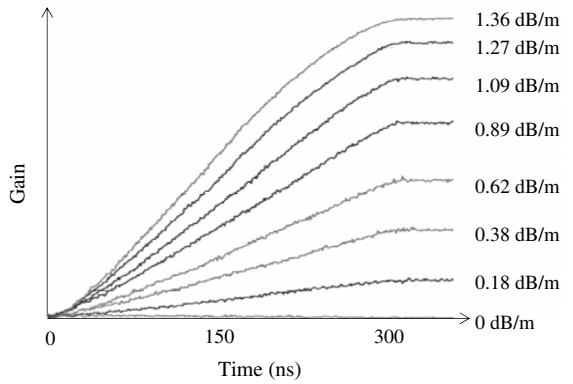

Fig. 4 Gain curve of the STC.

from a hard target can be measured in the turbid water without being affected by multiscattering. Specifically, the last signal is selected as the hard-target signal.

3 Experimental Result

To confirm the operation and the performance of the system, we performed a test in the pool of the Japan Agency for Marine-Earth Science and Technology, of 21 m (width) × 21 m (length) × 1.5 m (depth). Figure 5 shows the preliminary test setup in the pool. The system was set at a depth of 0.5 m, and two targets were set at about 4 and 8 m apart from the sensor. One of the targets is a painted board of size 1.5-m^2, and other one is a mannequin. The STC gain of 0.62 dB/m was used because the attenuation of the water in this pool was estimated to be about −0.7 dB/m. We manually tuned the gain curve of the STC at the beginning of the imaging experiments by predicting the attenuation in water using a turbidity meter. The automatic tuning is an issue for future work.

Figure 6 compares the 3-D image of the pool by switching the STC function on and off. The imaging frame rate and number of imaging pixels in this scanning condition are 0.2 Hz and 1080 (horizontal) × 214 (vertical). This corresponds to the pixel imaging rate of 46 kHz and seems to conflict with the above-mentioned pulse repetition rate of 50 kHz. This means there is some dead time for imaging.

To confirm the effect of the STC, we simulated low SNR conditions by setting the laser output power to 1% of the maximum possible output power. The x, y, and z indicate the width, height from pool floor, and length of the pool, respectively. The height from the floor of the pool is color-coded: blue is the floor of the pool and red is the highest point from the ground. The targets can be recognized as well as the structure of the pool, the floor, and the wall. The corner of the pool could be detected when the STC is on, whereas it could not be detected when it is off. These results show that the STC circuit improves the underwater performance.

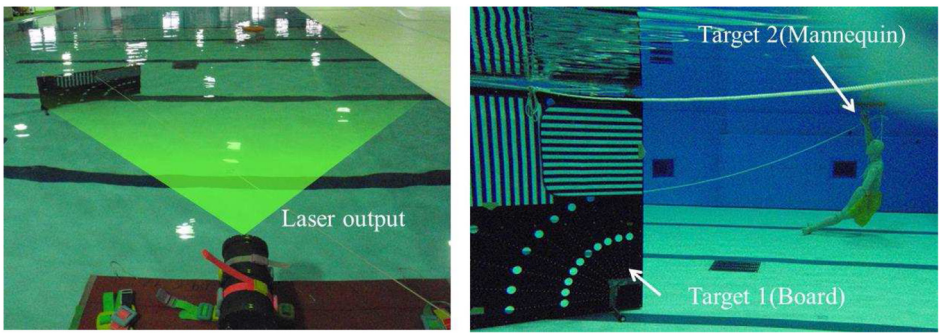

Fig. 5 Photograph of the preliminary test of 3-D imaging in the pool.

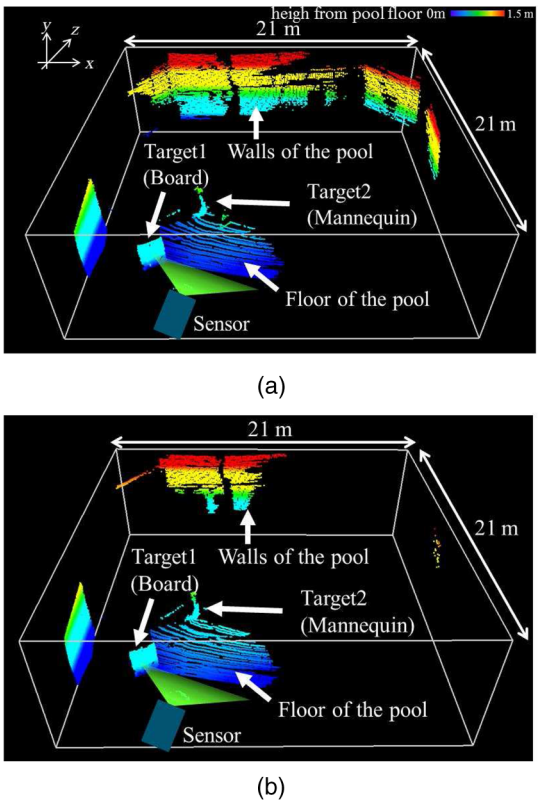

Fig. 6 3-D imaging of the pool: (a) STC function on and (b) STC function off. The height from ground is color-coded: blue is floor of the pool and red is high from the ground.

To estimate the measurement precision, we imaged the pool with the laser power set at 10% of the maximum. Figure 7 shows the 3-D image of the pool. The z is color-coded: blue is near, red is far from the sensor, and $z = 0$ is the sensor position. The reason for the stripped pattern (on the pool floor going in the z direction) is the different angle spacing of the beam spot between the horizontal and vertical directions. This angle spacing for the horizontal direction is 0.11 deg, and it is 0.14 deg for the vertical direction. It is seen that the spacing of strips becomes larger in the cases of shallower incident angles to the pool floor. This causes the stripped pattern. The measurement precision is estimated from the fluctuation of measurement distance to the wall, which is assumed at a constant distance. For this estimate, we used measured data from 100 points on the wall. Figure 8 shows the distance fluctuation at the wall. A standard deviation of 2.0 cm was obtained at a range of about 20 m. Note that this precision corresponds to the case of normal incidence of the laser beam to the target. This value can be reduced by averaging multiple images, since the fluctuation is caused by random noise. The standard deviation of the distance is written by

$$dZ \propto \frac{1}{\sqrt{N}}, \tag{3}$$

where N is the number of images. Concerning the distance accuracy, it is reasonable to consider that it is better than or equal to the half pulse length of the received target signal, since the signal detection is performed using a single threshold for the fall time of the last signal. This accuracy depends on the signal level and the received pulse length which

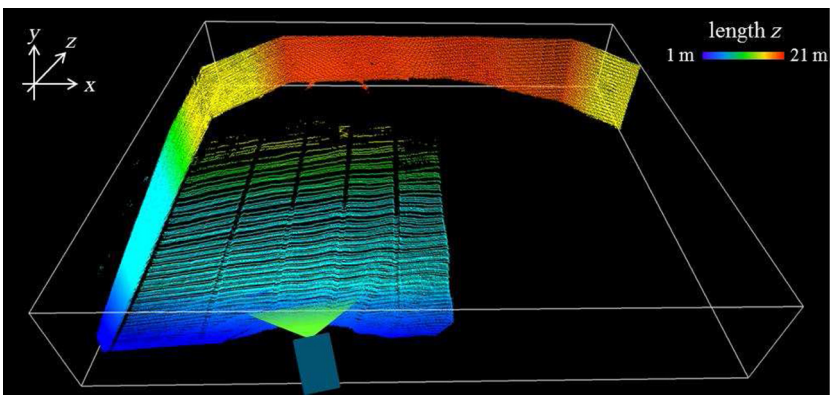

Fig. 7 3-D imaging of the pool. The distance z is color-coded: blue is near and red is far from the sensor.

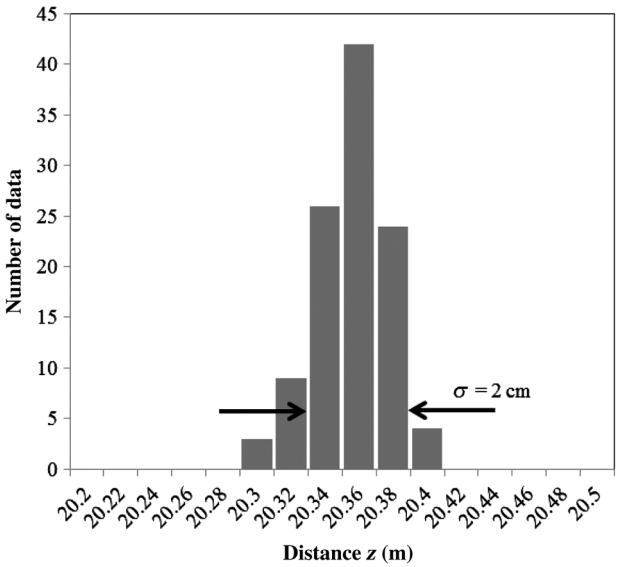

Fig. 8 Fluctuation of the measurement distance at the wall.

changes depending on the angle of incidence of the laser beam to the target. The detailed evaluation on the distance accuracy is also an issue for future work, in addition to the automatic tuning of the STC gain curve.

The received power from the target (W) and SNR (dB) of this system are written by

$$P_r(L) = P_t \cdot A_r \cdot \frac{1}{L^2} \cdot \eta \cdot \frac{\rho}{\pi} \exp\{-2 \int [a(L)] \mathrm{d}L\}, \tag{4}$$

$$\mathrm{SNR}(L) = 10 \log\left\{\frac{[Q \cdot M_p \cdot P_r(L)]^2}{2M_P^2 e\{[Q \cdot P_r(L)] + i_d\}B}\right\}, \tag{5}$$

where P_t is the output peak power (W), η is the total optical efficiency, α is the attenuation of the propagation medium (1/m), ρ is the reflectance of the target, assuming a Lambertian surface, L is the measurement distance of the line-of-sight (m), A_r is the aperture area of the receiver (m^2), Q is MCP-PMT cathode sensitivity (A/W), M_p is MCP-PMT gain, e is the elementary charge (C), i_d is MCP-PMT anode dark current (A), and B is the receiver bandwidth (Hz). Note that the influence of backscattering in the water is considered only in the attenuation but not in the received

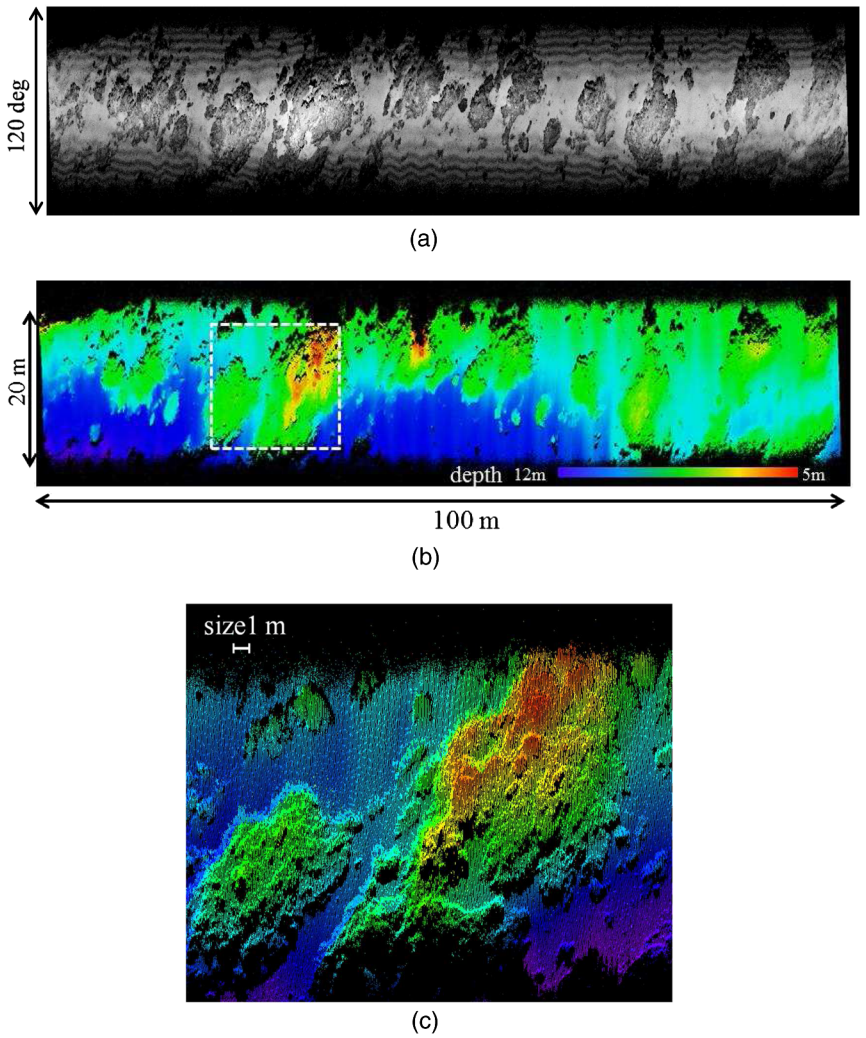

Fig. 9 Seafloor imaging results: (a) the intensity data, (b) the distance data from the sensor, and (c) the expanded 3-D image of the white dash area of the distance image.

power in Eq. (4). This is enough to study the signal detection ability for the target since we use the last signal detection as denoted in Sec. 2. Further, we ignore thermal noise in Eq. (5) because the shot noise and dark current noise are much larger than thermal noise due to the large gain of MCP-PMT. In this system, the aperture area of the receiver is 4.93×10^{-4} m^2, cathode sensitivity is 0.18 A/W, MCP-PMT gain is 70000, dark current is 3 nA, receiver bandwidth is 330 MHz, and optical efficiency is 0.4. For a wall reflectance of 1.0, reflections with 20 dB SNR can be obtained at 20 m distance, using 1% output laser power.

In addition, we performed a trial in a shallow water area around Ishigaki Island in December 2015 with full output laser power. This test was carried out on a small ship with the system hanging down into the sea. The image was measured with the beam scanning only in the horizontal direction and the scanning line spacing along with the direction of travel is derived by using the speed of the ship and the scanning rate. In this test, the number of imaging pixels for the horizontal direction, the scanning rate, and the speed of the ship are 2160 pixels, 22 Hz, and about 2 knot, respectively. This angle spacing for the horizontal direction is 0.056 deg, and scanning line spacing along with the direction of travel is 47 mm.

Figure 9 shows the seafloor imaging results: (a) is the intensity data, (b) is the distance data from the sensor, and (c) is the expanded 3-D image of the white dashed area of the distance image. The STC gain curve of 1.36 dB/m was used because the conditions in this field test were turbid, and the attenuation in the field was about 1.5 dB/m. In these conditions, the system could capture the shape of the undulating seafloor with submeter spatial resolution. Our results confirm that the system works well in field experiments in the ocean. The depth resolution is considered to be the same as the distance data precision of 2.0 cm by additionally assuming the ideal knowledge of the relative sensor position on the moving ship, although the output resolution of distance data is 4 mm which corresponds to the time resolution of TDC.

The received signal intensities, in the regions of top and bottom sides of the figure (i.e., the edge part of scanning), were relatively low because of the longer distance to the target and smaller solid angle for the receiving optics. There are some intensity ripples on the top and bottom sides. We supposed that this phenomenon was caused by the weak internal reflection of the transmitted pulse (at the optical devices in the sensor such as the dome lens, mirror, and lens) and the nonideal characteristics of the peak hold circuit. The current peak hold circuit is the simple capacitor type, as described in Sec. 2, and keeps the held voltage with a relatively long time (order of microseconds, corresponding to a distance of a few hundred meters). The pulse width is very short (1 ns), but the voltage holding continues for microseconds. This causes signal accumulation with (1) internal reflection, (2) backscattering in water, and (3) target signal. The influence of this accumulation becomes relatively distinct when the level of the target signal becomes low. If the level of the internal reflection has an angle dependence, this causes the above-mentioned ripples in the intensity map.

4 Summary

We developed an underwater 3-D imaging sensor using a 532-nm laser. Our system uses a dome lens and coaxial optics to realize a wide-scanning angle of 120 deg (horizontal) × 30 deg (vertical) while having a compact size of 25-cm diameter and 60-cm length.

The key feature of this sensor is the wide-scanning angle combined with pressure resistance and compactness. This feature is realized by the combination of the dome lens, the coaxial optics, and an optical design that avoids internal light reflections. This system also has an STC circuit which enables the detection of smaller signals.

The performance of the sensor was confirmed in pool tests, and we demonstrated the 3-D imaging in field experiments in the ocean. The results of the field experiments indicate that our sensor exhibits significant potential for underwater exploration using AUVs and ROVs.

References

1. H. Yoshida et al., "The 3-D scanning laser installed on an underwater vehicle achieves observation of seafloor," in *Proc. of the 11th SEGJ Int. Symp.*, pp. 362–364 (2013).
2. S. Ishibashi and H. Yoshida, "An optical visualization technology applied to unmanned underwater vehicles," in *The Twenty-Fifth Int. Offshore and Polar Engineering Conf. Int. Society of Offshore and Polar Engineers* (2015).
3. J. S. Jaffe, "Computer modeling and the design of optimal underwater imaging systems," *IEEE J. Oceanic Eng.* **15**, 101–111 (1990).
4. E. Kaltenbacher et al., "Development of a compact, real-time, optical system for 3-D mapping of the ocean floor (invited)," in *Proc. Oceanology Int.* (2001).
5. C. Roman, G. Inglis, and J. Rutter, "Application of structured light imaging for high resolution mapping of underwater archaeological sites," in *OCEANS 2010 IEEE-Sydney*, pp. 1–9 (2010).
6. A. Bodenmann, B. Thornton, and T. Ura, "Development of long range color imaging for wide area 3D reconstructions of the seafloor," in *2013 IEEE Int. Underwater Technology Symp.*, pp. 1–5 (2013).
7. F. R. Dalgleish, "An AUV-deployable pulsed laser line scan (PLLS) imaging sensor," in *Proc. Oceans 2007*, pp. 1–5 (2007).
8. C. Embry et al., "Subsea monitoring—high resolution 3D laser imaging for inspection, maintenance, repair, and operations," in *Proc. the Offshore Technology Conf.* (2012).
9. D. Richardson et al., "High resolution 3D laser imaging for inspection, maintenance, repair, and operations," in *Proc. the Offshore Technology Conf.* (2013).
10. T. Reees et al., "AUV-based 3D laser inspection for structural integrity management in deepwater fields," in *Offshore Technology Conf. Offshore Technology Conf.* (2014).
11. N. G. Jerlov, *Marine Optics*, p. 23, Elsevier, Amsterdam Netherlantds (1976).

Masaharu Imaki received his DE degree from the University of Fukui in 2005. He has been involved in the development of Doppler lidar, Raman lidar, differential absorption lidar (DIAL), and high-spectral resolution lidar in the university. In 2007, he joined Mitsubishi Electric Corporation. His current research involves distance imaging sensors, DIAL, and Doppler lidar. He is a member of SPIE, the Japan Society of Applied Physics, the Laser Society of Japan, and the Institute of Electrical Engineers of Japan.

Hideaki Ochimizu received his MS degree from the University of Tokyo, Japan, in 2008. He joined Mitsubishi Electric Corporation in 2008 and worked on projects of electro-optics sensor systems, especially infrared sensors and laser application. Since 2016, he has been a visiting researcher at Mitsubishi Electric Research Laboratories. His research interests are LIDAR and signal processing for 3-D point cloud. He is a member of the Japan Society of Applied Physics.

Hidenobu Tsuji received his BS and MS degrees in physics from the Tokyo Institute of Technology in 2004 and 2006, respectively, and his PhD in science from the Tokyo Institute of Technology in 2011. He is a head researcher at Mitsubishi Electric Corporation. His current research interests include optics about laser sensor and laser sensor systems.

Shumpei Kameyama received his DE degree from Chiba University in 2011. Since 1995, he has been with the Mitsubishi Electric Corporation, and he started the development of laser remote sensing systems in 1999. His current research involves coherent Doppler

lidar, differential absorption lidar, and range imaging laser sensors. He is a member of the Japan Society of Applied Physics, Optical Society of America, and Institute of Electrical and Electronics Engineers.

Takashi Saito has been a manager in Market Planning and Administration Center, Mitsubishi Electric TOKKI Systems Corporation, since he joined in 1983. He was engaged in research and development of radar, terrestrial radio, and millimeter wave radio systems from 1983 to 2005. He is currently engaged in research and development of underwater laser and underwater acoustic communication systems.

Shojiro Ishibashi received his PhD from the Tokyo University of Mercantile Marine in 2003. He belongs to Japan Agency for Marine Earth Science and Technology (JAMSTEC) as an engineering researcher from 2003. His specialty is underwater vehicle technology including relating technologies. Recently, he is very interested in underwater optical technology in order to apply to an underwater vehicle. He is a member of the JSME, JIME, AMSTEC, and SEGJ.

Hiroshi Yoshida received his Dr. degree in physics from Kanazawa University, Japan. He has been studying underwater vehicle technologies for the past 10 years and has led efforts to apply the technology for a variety of applications. His current interests include R&D of unmanned underwater vehicles as well as underwater electromagnetics.